NANOELECTRONICS

End-bonded contacts for carbon nanotube transistors with low, size-independent resistance

Qing Cao,* Shu-Jen Han, Jerry Tersoff, Aaron D. Franklin,† Yu Zhu, Zhen Zhang,‡ George S. Tulevski, Jianshi Tang, Wilfried Haensch

Moving beyond the limits of silicon transistors requires both a high-performance channel and high-quality electrical contacts. Carbon nanotubes provide high-performance channels below 10 nanometers, but as with silicon, the increase in contact resistance with decreasing size becomes a major performance roadblock. We report a single-walled carbon nanotube (SWNT) transistor technology with an end-bonded contact scheme that leads to size-independent contact resistance to overcome the scaling limits of conventional side-bonded or planar contact schemes. A high-performance SWNT transistor was fabricated with a sub–10-nanometer contact length, showing a device resistance below 36 kilohms and on-current above 15 microampere per tube. The p-type end-bonded contact, formed through the reaction of molybdenum with the SWNT to form carbide, also exhibited no Schottky barrier. This strategy promises high-performance SWNT transistors, enabling future ultimately scaled device technologies.

After decades of rapidly increasing computer performance, microprocessor clock frequencies have stalled at ~3 to 5 GHz since the early 2000s, as silicon (Si) metal-oxide-semiconductor field-effect transistors (MOSFETs) approach their physical limits (*1*–*3*). Two key issues are making high-performance but low-power devices with ultrashort gate pitch (the summary of channel length L_{ch}, the distance between the source and drain electrodes, and the contact length L_c, the length of these contacts)—that is, less than 30 to 40 nm—and lowering the contact resistance between the electrodes and the channel. The problems are interrelated, in that contact resistance increases with decreasing L_c for Si and especially for III-V semiconductors such as GaAs (*2*, *4*). Semiconducting single-walled carbon nanotubes (SWNTs) potentially offer the optimal performance as the channel material for ultrascaled FETs (*5*–*7*). The SWNT saturation velocity is several times higher than that of Si, and the intrinsic thinness (~1 nm in diameter) of SWNTs provides the superior electrostatic control needed for devices with ultrashort L_{ch} (*6*). Indeed, SWNT transistors with 9 nm L_{ch} outperform the best Si MOSFETs with similar L_{ch} (*8*, *9*), and SWNT transistors with advanced self-aligned "gate-all-around" geometry have been fabricated (*10*, *11*) and integrated into complex functional integrated circuits (*12*, *13*).

However, as is the case with Si and III-V semiconductors, a key obstacle to ultrascaled SWNT transistor technology is forming low-resistance and scalable contacts. The total contact resistance $2R_c$ dominates the performance of scaled devices as the channel transport becomes ballistic. Early SWNT transistors were plagued by poor electrical properties of the metal contacts (*14*, *15*). In a major advance, Javey *et al.* achieved low-resistance barrier-free p-type electrical contacts to SWNT using palladium (Pd) (*16*). As in earlier work, the Pd metal was deposited on top of the SWNT to form so-called side-bonded contacts, in which electrons are injected along the length of the tube-metal interface (*15*, *17*). However, with such a contact scheme, $2R_c$ is low only for large-area contacts, reflecting the weak Pd-SWNT coupling, and the resistance $2R_c$ increases rapidly as the contact area shrinks (*18*–*20*). [The weak metal-SWNT coupling is not well understood and might reflect the nonideal wetting of metals on a curved nanotube surface, or the partial coverage of nanotube surface by insulating impurities such as amorphous carbon (C)]. The contact area is proportional to L_c measured along the SWNT direction. Previous experiments indicate that $2R_c$ will increase from ~5 kilohm for long contacts (L_c > 200 nm) to ~65 kilohm at L_c of 9 nm (*21*), and to much higher values for even smaller contacts, which is unacceptably large for logic transistors beyond the 2020 time frame (*22*).

Here, we report a contact scheme that allows scaling the contacts to 10 nm and beyond without increasing $2R_c$. An end-bonded contact, in which the SWNT channel abruptly ends at the metal electrodes, is formed through a solid-state reaction between the nanotube and deposited Mo electrodes. Although the carrier injection is limited to an interface of ~2 nm^2 in size, $2R_c$ was remarkably low, down to 25 to 35 kilohm. No barrier was observed for hole transport, and scaling L_c from 300 nm to below 10 nm did not change the contact resistance; whereas in conventional side-bonded contacts to nanotubes or planar contacts in Si MOSFETs, $2R_c$ shows a characteristic dependence on L_c. Using this end-bonded contact scheme, we successfully demonstrate a p-channel SWNT transistor with an average contact length of merely 9 nm that exhibits on-state

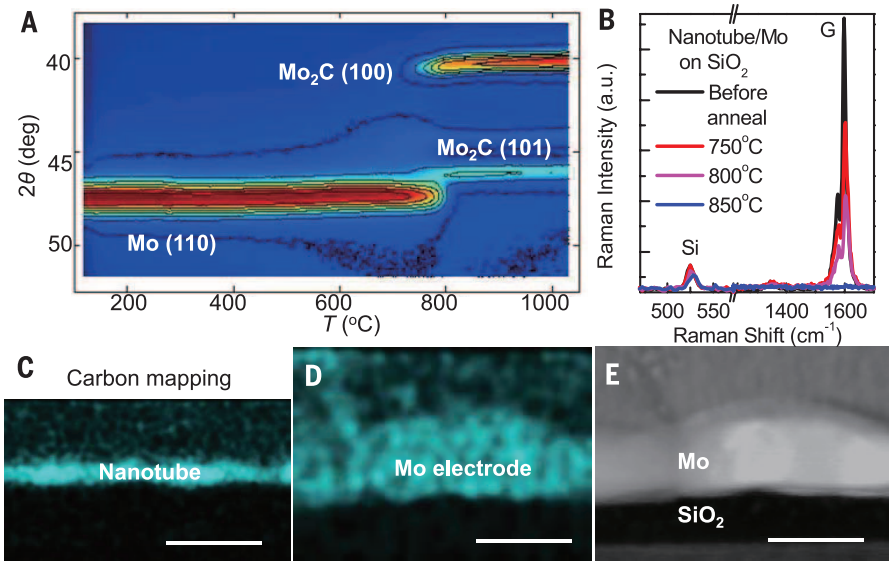

Fig. 1. Reaction of carbon nanotubes with Mo thin film. (**A**) In situ temperature-variable x-ray diffraction pattern of Mo deposited on a thick nanotube film showing peaks characteristics for Mo and Mo_2C. (**B**) Raman spectra for double-layered nanotubes covered by 8 nm Mo before and after annealed under difference temperatures, showing the characteristic G band of nanotubes and the transverse optical phonon band of crystalline Si substrate. (**C** and **D**) False-colored EDX maps of carbon for nanotubes annealed to 850°C without (part C) or with (part D) the Mo film on top. (**E**) Cross-sectional TEM image showing the profile of the Mo film after annealing as in (D). Scale bars, 20 nm.

IBM Thomas J. Watson Research Center, Yorktown Heights, NY 10598, USA.
*Corresponding author. E-mail: qcao@us.ibm.com †Present address: Department of Electrical and Computer Engineering, Duke University, Durham, NC 27708, USA. ‡Present address: Department of Engineering Sciences, Uppsala University, Uppsala, Sweden.

resistance below 36 kilohm, an on/off current ratio above 10^4, an on-current above 15 μA, and a zero Schottky barrier at contacts.

Ab initio calculations suggest that SWNTs could form good electrical contacts to metals in the end-bonded geometry in which an open tip of the nanotube is directly coupled to metal electrodes through strong covalent bonds (*23*–*25*). However, it is very difficult to realize such a structure in experiment. Zhang *et al.* reported the fabrication of SWNT-metal heterostructures through the solid-state carbide formation reaction, in which the C-C bond cleavage and the C-metal bond formation were completed simultaneously (*26*). The atomically abrupt metal-nanotube junctions have been characterized by means of transmission electron microscopy (TEM) for metals including titanium (Ti) and niobium (Nb) (*26*), as well as tungsten (W), iron (Fe), and chromium (Cr) (*27*, *28*). However, their successful adoption in transistors as reliable low-resistance contacts has not yet been demonstrated because of integration challenges. The best attempt to date used Ti (*29*), but Ti is problematic because its low work function leads to a Schottky barrier (*29*, *30*), and destructive reactions with the gate oxide occur at the carbide formation temperature (*31*). Fifteen metals are known to form stable carbide phases (*32*), and among these, W, molybdenum (Mo), and Fe exhibit the highest electronegativity or work function and thus have the strongest tendency to form carbides rather than oxides. Among these three candidates, WC requires formation temperature well above 1000°C, whereas in Fe_3C, a graphite layer is generally observed to segregate atop (*32*). Thus, we believe that Mo_2C is the best candidate for contacting semiconducting SWNTs.

We confirmed the reaction between carbon nanotubes and the deposited Mo film using time-resolved in situ x-ray diffraction (XRD) (Fig. 1A). To obtain sufficient XRD signal intensity, a thick Mo film (30 nm) was deposited on top of a 200-nm-thick mat of SWNTs sitting on a SiO_2/Si substrate (*33*). The C atoms from the SWNTs started to react with Mo to form Mo_2C above ~800°C, as evidenced by the disappearance of Mo (110) peak around $2\theta \approx 47°$ and the emergence of carbide peaks at $2\theta \approx 40°$ and 46°, which correspond to the (100) and (101) planes of the Mo_2C crystal, respectively. In real devices, the amount of C provided by SWNTs is much smaller than the Mo available in the electrodes. To verify the reaction in this regime, Raman spectroscopy was used to monitor the effect of thermal treatment on a bilayer of SWNTs [~4 nm thick, assembled with the Langmuir-Schaefer method (*34*)] covered by a semitransparent 8-nm-thick Mo film. Although the structural integrity of exposed SWNTs was not affected in this temperature range under vacuum (fig. S1), the Raman intensity of the characteristic G band of the nanotubes under Mo started to decrease above 750°C and was completely extinguished in samples annealed at 850°C (Fig. 1B), indicating the occurrence of a reaction destroying the SWNT lattice. Energy-dispersive x-ray (EDX) spectroscopy mapping revealed that under the Mo, the C atoms from the SWNTs dispersed into the Mo (Fig. 1, C to E). In a real device structure in which SWNTs are only covered by Mo in the contact region, this dissolution of C in Mo matrix should lead to an abrupt point-like junction between the three-dimensional (3D) Mo electrode and the 1D SWNT channel (Fig. 2, A to B), considering the low diffusion coefficient of Mo resulting from its high melting temperature (*26*).

Forming such desired end-bonded structure does not guarantee the good electrical quality of the contacts between Mo and the semiconducting SWNT channel. In order to qualify as a good electrical contact, this pointlike Mo-SWNT end contact must exhibit nearly zero barrier and small contact resistance even with a cross-sectional area down to ~1 nm^2. To test this, Mo end-contacted FETs with a nominal L_{ch} of 60 nm were made with individual SWNTs deposited from solution. These devices have rather large Mo electrodes (~500 nm wide) and were fabricated on a Si substrate covered by 20 nm thermally robust Si nitride gate dielectric. The transfer characteristics of a representative device are shown in Fig. 2C,

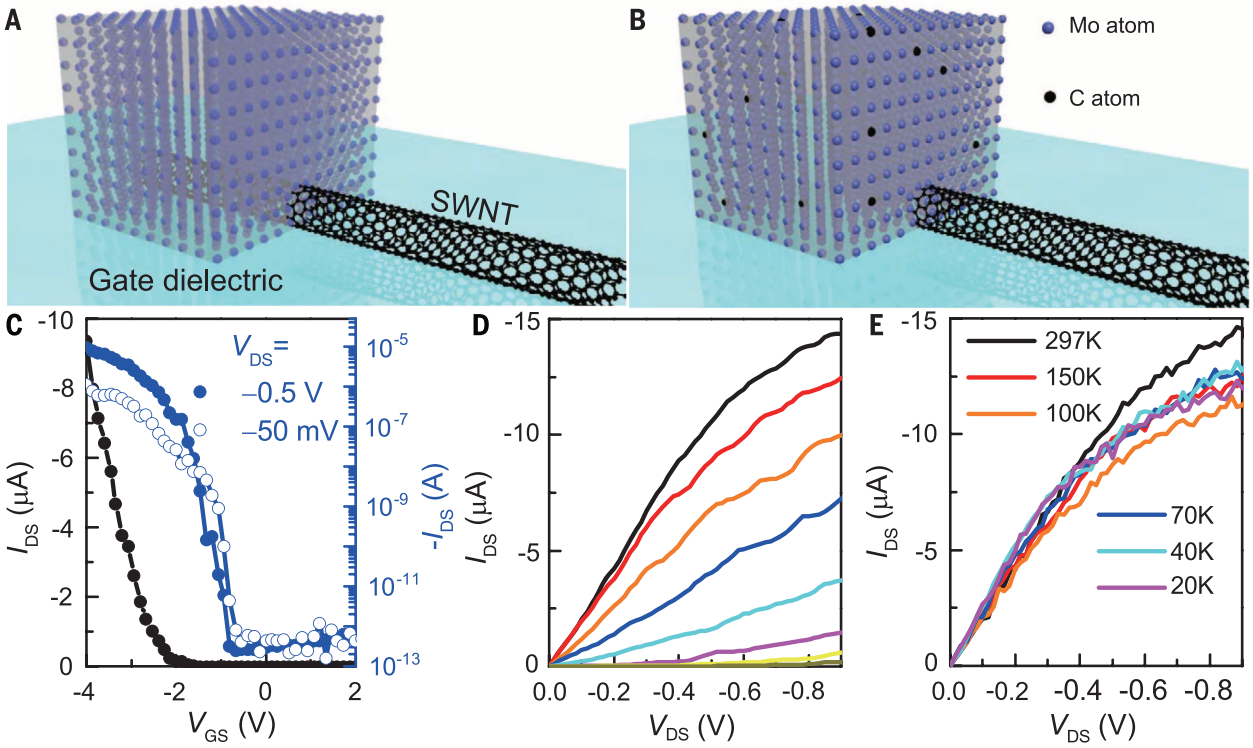

Fig. 2. Mo end-contacted SWNT transistors. (**A** and **B**) Schematics showing the conversion from a side-bonded contact (A), where the SWNT is partially covered by Mo, to end-bonded contact (B), where the SWNT is attached to the bulk Mo electrode through carbide bonds while the C atoms from originally covered portion of the SWNT uniformly diffuse out into the Mo electrode. (**C**) Transfer characteristics of a typical Mo end-contacted single-nanotube transistor built on 20 nm SiN_x gate dielectric with a nominal L_{ch} of 60 nm plotted in both linear (black, left axis) and logarithmic (blue, right axis) scales with applied V_{DS} of −0.5 V (filled circles) and −0.05 V (hollow circles). I_{DS}, drain-to-source current. (**D**) Output characteristics of the device at room temperature (V_{GS} changes from −6 V to 1 V in steps of 1 V). (**E**) Output characteristics for the same device taken at V_{GS} = −6 V for different temperatures ranging from 297 to 20 K.

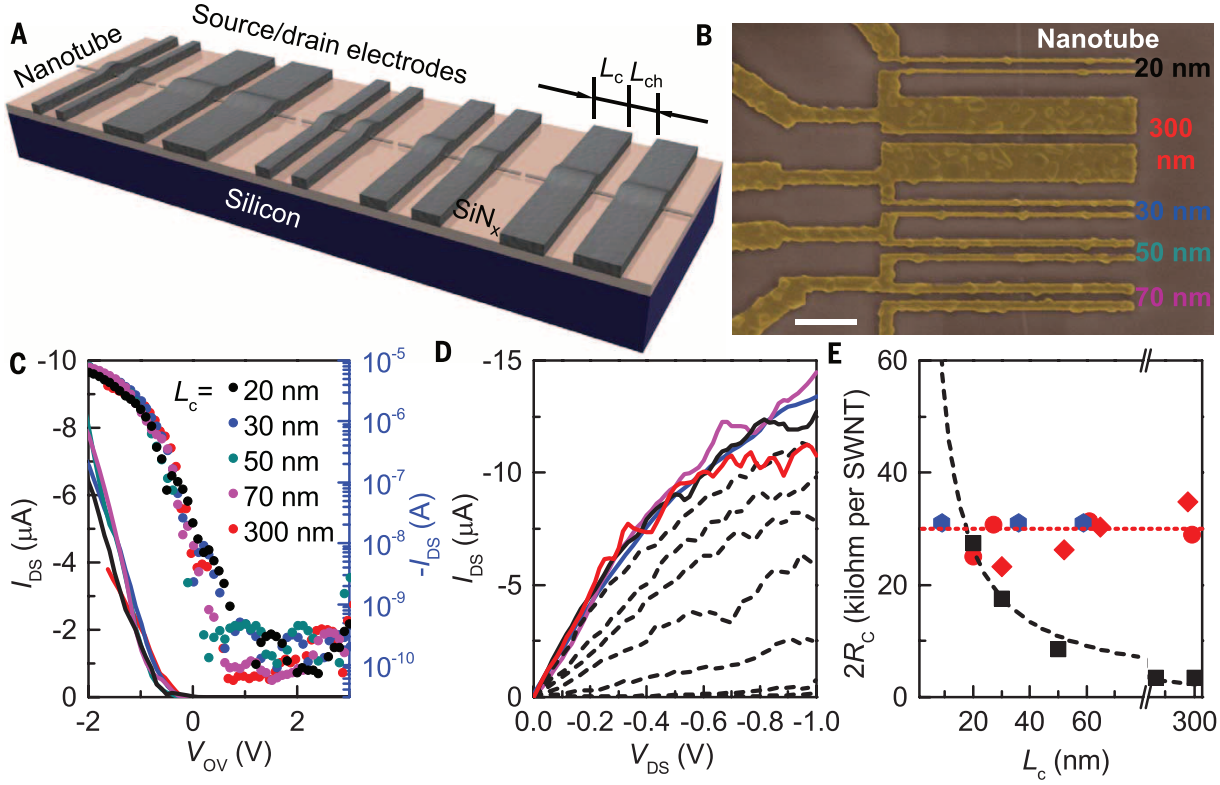

Fig. 3. Contact length scaling of Mo end-contacted quasiballistic SWNT transistors. (**A**) Schematic and (**B**) false-colored SEM images of a set of transistors fabricated on the same nanotube, with L_c ranging from 20 to 300 nm. Scale bar, 400 nm. (**C**) Collection of transfer characteristics from a set of Mo end-contacted single-nanotube transistors with different L_c plotted in both linear (lines, left axis) and logarithmic (symbols, right axis) scales with applied V_{DS} of −0.5 V. (**D**) Output characteristics of the same devices as in (C) measured at V_{GS} of −6 V. Curves for the device with 20 nm L_c measured with descending V_{GS} at a step of 1 V are also plotted (dashed lines). (**E**) Plot of $2R_c$ as a function of L_c for two sets of Mo end-contacted devices (red), with each set on a different nanotube (red circle or diamond represents a set of transistors on the same tube), and the best Pd side-contacted nanotube devices from (*21*) (black square). Additional Mo end-contacted nanotube devices whose L_c are confined by contact trenches (extracted from Fig. 4F) are shown as blue hexagons. The black dashed curve represents a fitting to the formula of $2R_c = 2\rho_c/L_c$, where ρ_c is the linear contact resistivity. The red dotted line serves as a visual guide highlighting the invariance of $2R_c$ for end-bonded contacts.

with an on/off current ratio up to 10^7 and a small subthreshold swing of ~100 mV/decade. Its output characteristics (Fig. 2D) reveal other aspects of the excellent device performance, including on-state resistance ~40 kilohm, saturation current near 15 μA, and nearly linear current-voltage characteristics at small drain-to-source bias (V_{DS}). All of these results suggest that high-quality barrier-free contacts were formed. The absence of Schottky barrier was further confirmed with temperature-dependent measurements. The device output characteristics remain unchanged when measured from room temperature to 20 K (Fig. 2E), indicating nearly zero Schottky barrier for hole injection. Although the real contact area is extremely small, these end-bonded contacts demonstrate excellent electrical reliability, with negligible changes in on-state current or on/off current ratio when the device was electrically cycled more than 400 times, under a peak current density above 4×10^8 A cm^{-2} (fig. S2), presumably because of the formation of robust metal carbide bonds (*28*).

For truly end-bonded contacts, $2R_c$ should be independent of contact size. Unlike conventional side contacts, all of the carrier collection should occur at the quasi-0-D interface, with the negligible spreading resistance (fig. S3) (*33*), so the contact resistance $2R_c$ should be independent of the physical width of the metal contact L_c. We measured devices with a short L_c of 20 nm made on solution-processed SWNTs and found that ~50% of them exhibited low overall device resistance (below 40 kilohm) (fig. S4), which is comparable with the ratio obtained from devices made with wide contacts. To further confirm the invariance of contact resistance with L_c and verify the formation of an end-bonded contact, we needed to control other factors, in particular the dependence of $2R_c$ on the SWNT diameter and band gap (*16*). To do this, we fabricated a series of devices with different L_c on the same long nanotube grown by means of chemical vapor deposition (Fig. 3, A and B). This approach provided precisely defined device geometries with a constant diameter and band gap among devices. The diameter of this particular SWNT was ~1.6 nm (fig. S5) from atomic force microcopy (AFM). The L_{ch} for each device was 60 nm, so that the SWNT channel should be ballistic, and thus the $2R_c$ could be approximated as the total device resistance minus the quantum resistance of the SWNT channel (R_Q = 6.5 kilohm) (*16*).

The transfer characteristics of devices with L_c varying from 20 to 300 nm at the same gate overdrive (V_{OV}, defined as the gate bias V_{GS} applied above the device threshold voltage) (plotted in Fig. 3C) showed no off-state performance difference caused by such wide L_c variation. The values of $2R_c$, extracted from the low-field slope of the output curves at high V_{GS} (Fig. 3D), are all in the range of 25 to 35 kilohm per SWNT. Considering that the junction area is merely ~2 nm^2, this value corresponds to a contact resistivity as low as 3×10^{-10} ohm cm^2, compared with previous best value in the range of 1.5×10^{-9} to 4×10^{-9} ohm cm^2 for metal to Si or SWNT contacts (*21*, *35*). In Fig. 3E, the L_c scaling of our devices is compared with one of the best reported Pd side-bonded contacts (*21*). For side-bonded contacts, because of the distributed nature of SWNT-metal interface, the $2R_c$ is proportional to the reciprocal of L_c in small contact regime as in the standard transmission line model commonly used for semiconductor devices (*19*, *36*). Mo end-bonded contacts start to outperform Pd side-bonded contacts at dimensions near 20 nm, and we project that the former possesses more than two times the performance advantage for L_c scaled below 10 nm.

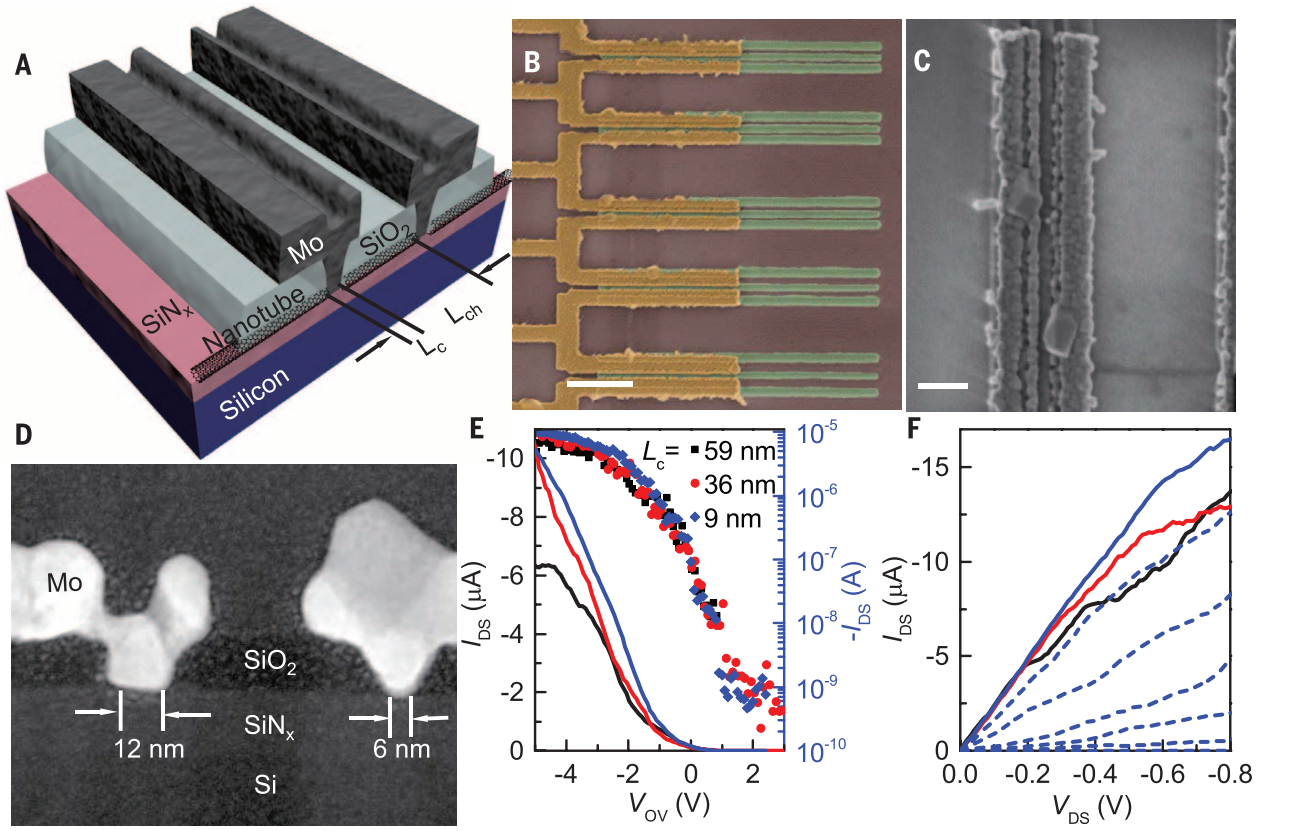

Fig. 4. Mo end-contacted quasiballistic SWNT transistors with L_c defined by contact trenches. (**A**) Schematic and (**B**) false-colored SEM image of a set of Mo end-contacted nanotube transistors made on the same nanotube with L_c ranging from ~10 to 60 nm defined by SiO_2 contact trenches. The diameter of this particular nanotube is determined to be ~1.7 nm by means of AFM (fig. S5). Scale bar, 400 nm. (**C**) Top-view SEM image of the ~9 nm effective L_c nanotube transistor at a higher magnification. Scale bar, 100 nm. (**D**) Cross-sectional high-angle annular dark field-STEM of this device showing the trench profile for the accurate determination of L_c. (**E**) Collection of transfer characteristics from the set of Mo-contacted nanotube transistors as in (B) with different L_c plotted in both linear (lines, left axis) and logarithmic (symbols, right axis) scales under applied V_{DS} of −0.5 V. (**F**) Output characteristics of the same devices as in (E) measured at V_{OV} of −7 V. Curves for the device with ~9 nm effective L_c measured with descending V_{GS} at a step of 1 V are also plotted (dashed lines).

As a final demonstration that a Mo end-bonded contact can maintain its low $2R_c$ and thus serve as the contact scaling solution for future ultimately scaled device technologies, we constructed a SWNT transistor with a physical L_c below 10 nm (a schematic is shown in Fig. 4A; the detailed fabrication flow is depicted in fig. S6). The actual Mo-to-SWNT contacts are confined by the size of SiO_2 trenches, similar to the contact vias in standard Si MOSFETs. The corresponding scanning electron microscopy (SEM) and scanning transmission electron microscopy (STEM) images in Fig. 4, B to D, characterize the geometry of the sub–10-nm L_c device, performed after electrical measurements. The cross-sectional STEM image (Fig. 4D) provides information on the sidewall shape of the SiO_2 trenches to give an accurate extraction of the effective device L_c to be ~9 nm, which is taken as the average of L_c for source and drain electrodes. Mo nicely filled into these narrow vias. The roughness on the metal top surface is caused by the grain growth induced by this annealing process and can be planarized with a chemical-mechanical polishing process in the real technology integration process flow. Transfer and output characteristics of three devices with effective L_c of 59, 36, and 9 nm made on this SWNT are plotted in Fig. 4, E and F, with their on-current levels consistent with each other, confirming the L_c independence of $2R_c$ (Fig. 3E). The device with 9 nm L_c performs well with an on-current of >10 μA at only −0.5 V V_{DS}, an on/off current ratio of 10^4, and extracted overall device resistance in low-bias regime less than 36 kilohm. For a realistic SWNT transistor consisting of a nanotube array with a tube pitch of ~8 nm (*5*), the effective device contact resistance per width becomes ~240 ohm μm, which satisfies even the most stringent target listed by International Roadmap for Semiconductors up to 1.3 nm technology node in 2028 (*37*). This end-bonded contact geometry formed through reaction between Mo and nanostructures could readily be extended to improve the L_c scaling behavior of ultrascaled nanoelectronic devices on the basis of other low-dimensional materials including graphene and MoS_2. We have only demonstrated p-channel SWNT transistors using p-type end contacts. It will be difficult to form end-bonded n-type contacts to SWNTs in which electrons are directly injected into the conduction band of SWNTs with this carbide formation approach, as metals with low enough work function tend to oxidize first rather than react with C. However, it is still possible to realize n-channel SWNT device operation even with end-bonded contacts to high work function metals through electrostatic doping in the vicinity of the source electrode (*10*, *38*).

REFERENCES AND NOTES

1. T. N. Theis, P. M. Solomon, *Science* **327**, 1600–1601 (2010).
2. W. Haensch *et al.*, *IBM J. Res. Develop.* **50**, 339–361 (2006).
3. R. F. Service, *Science* **323**, 1000–1002 (2009).
4. J. A. del Alamo, *Nature* **479**, 317–323 (2011).
5. G. S. Tulevski *et al.*, *ACS Nano* **8**, 8730–8745 (2014).
6. J. Appenzeller, *Proc. IEEE* **96**, 201–211 (2008).
7. A. D. Franklin, *Nature* **498**, 443–444 (2013).
8. A. D. Franklin *et al.*, *Nano Lett.* **12**, 758–762 (2012).
9. F. Kreupl, *Nature* **484**, 321–322 (2012).
10. A. D. Franklin *et al.*, *Nano Lett.* **13**, 2490–2495 (2013).
11. C. D. Cress, S. Datta, *Science* **341**, 140–141 (2013).
12. Q. Cao *et al.*, *Nature* **454**, 495–500 (2008).
13. M. M. Shulaker *et al.*, *Nature* **501**, 526–530 (2013).
14. J. Appenzeller *et al.*, *Phys. Rev. Lett.* **89**, 126801 (2002).
15. F. Léonard, A. A. Talin, *Nat. Nanotechnol.* **6**, 773–783 (2011).
16. A. Javey, J. Guo, Q. Wang, M. Lundstrom, H. Dai, *Nature* **424**, 654–657 (2003).
17. N. Nemec, D. Tománek, G. Cuniberti, *Phys. Rev. Lett.* **96**, 076802 (2006).

18. F. Xia, V. Perebeinos, Y. M. Lin, Y. Wu, P. Avouris, *Nat. Nanotechnol.* **6**, 179–184 (2011).
19. P. M. Solomon, *IEEE Electron Device Lett.* **32**, 246–248 (2011).
20. A. D. Franklin, D. B. Farmer, W. Haensch, *ACS Nano* **8**, 7333–7339 (2014).
21. A. D. Franklin, Z. Chen, *Nat. Nanotechnol.* **5**, 858–862 (2010).
22. International technology roadmap for semiconductors (ITRS, www.itrs.net) predicts that the device L_{ch} should shrink to ~10 nm by the 2020 time frame, with length of ~9 nm for contacts. For a realistic carbon nanotube transistor consisting of a nanotube array with a tube pitch of ~8 nm, when scaled to L_c of 9 nm the effective device contact resistance per width for best side-bonded Pd contacts becomes ~520 ohm μm, which is two to three times higher than that of current silicon MOSFETs.
23. J. J. Palacios, A. J. Pérez-Jiménez, E. Louis, E. SanFabián, J. A. Vergés, *Phys. Rev. Lett.* **90**, 106801 (2003).
24. V. Vitale, A. Curioni, W. Andreoni, *J. Am. Chem. Soc.* **130**, 5848–5849 (2008).
25. Y. Matsuda, W.-Q. Deng, W. A. Goddard III, *J. Phys. Chem. C* **114**, 17845–17850 (2010).
26. Y. Zhang, T. Ichihashi, E. Landree, F. Nihey, S. Iijima, *Science* **285**, 1719–1722 (1999).
27. J. A. Rodríguez-Manzo *et al.*, *Proc. Natl. Acad. Sci. U.S.A.* **106**, 4591–4595 (2009).
28. M.-S. Wang, D. Golberg, Y. Bando, *Adv. Mater.* **22**, 5350–5355 (2010).
29. R. Martel *et al.*, *Phys. Rev. Lett.* **87**, 256805 (2001).
30. Z. Chen, J. Appenzeller, J. Knoch, Y. M. Lin, P. Avouris, *Nano Lett.* **5**, 1497–1502 (2005).
31. A. E. Morgan, E. K. Broadbent, K. N. Ritz, D. K. Sadana, B. J. Burrow, *J. Appl. Phys.* **64**, 344–353 (1988).
32. W. P. Leroy, C. Detavernier, R. L. Van Meirhaeghe, C. Lavoie, *J. Appl. Phys.* **101**, 053714 (2007).
33. Materials and methods are available as supplementary materials on *Science* Online.
34. Q. Cao *et al.*, *Nat. Nanotechnol.* **8**, 180–186 (2013).
35. Z. Zhen *et al.*, *IEEE Electron Device Lett.* **34**, 723–725 (2013).
36. K. L. Grosse, M.-H. Bae, F. Lian, E. Pop, W. P. King, *Nat. Nanotechnol.* **6**, 287–290 (2011).
37. ITRS predicts that overall source/drain parasitic resistance per width should be 256 ohm μm for multigate transistors targeting at high-performance applications at 1.3 nm technology node with a L_c less than 4 nm in 2028. However, no manufacturable solutions are known to keep this resistance level upon scaling beyond even a 7-nm node from 2018.
38. J. Zhang, C. Wang, Y. Fu, Y. Che, C. Zhou, *ACS Nano* **5**, 3284–3292 (2011).

ACKNOWLEDGMENTS

We thank J. Bucchignano for technical assistance with electron-beam lithography. Q. C. conceived and designed the experiments. Q.C., S.-J.H., A.D.F., and J.S.T. performed the experiments. Y.Z. performed STEM and EDX analysis. Z.Z. performed in situ XRD. G.S.T. provided carbon nanotubes. Q.C. wrote the manuscript. All authors discussed the results and commented on the manuscript.

SUPPLEMENTARY MATERIALS

www.sciencemag.org/content/350/6256/68/suppl/DC1
Materials and Methods
Figs. S1 to S7
References (*39*–*43*)

15 June 2015; accepted 4 August 2015
10.1126/science.aac8006

POLYMER CHEMISTRY

Megasupramolecules for safer, cleaner fuel by end association of long telechelic polymers

Ming-Hsin Wei,[1]* Boyu Li,[1]* R. L. Ameri David,[1] Simon C. Jones,[2] Virendra Sarohia,[3] Joel A. Schmitigal,[4] Julia A. Kornfield[1]†

We used statistical mechanics to design polymers that defy conventional wisdom by self-assembling into "megasupramolecules" (≥5000 kg/mol) at low concentration (≤0.3 weight percent). Theoretical treatment of the distribution of individual subunits—end-functional polymers—among cyclic and linear supramolecules (ring-chain equilibrium) predicts that megasupramolecules can form at low total polymer concentration if, and only if, the backbones are long (>400 kg/mol) and end-association strength is optimal. Viscometry and scattering measurements of long telechelic polymers having polycyclooctadiene backbones and acid or amine end groups verify the formation of megasupramolecules. They control misting and reduce drag in the same manner as ultralong covalent polymers. With individual building blocks short enough to avoid hydrodynamic chain scission (weight-average molecular weights of 400 to 1000 kg/mol) and reversible linkages that protect covalent bonds, these megasupramolecules overcome the obstacles of shear degradation and engine incompatibility.

Ultralong polymers (weight-average molecular weight $M_w \geq 5000$ kg/mol) exhibit striking effects on fluid dynamics even at low concentration; for example, polymer concentrations of 100 parts per million (ppm) or less can enable mist control (*1*, *2*) and drag reduction (*3*). The key to both mist control and drag reduction is the ability of polymers to store energy as they stretch, such that the fluid as a whole resists elongation. The high potency of ultralong linear polymers is due to the onset of chain stretching at low elongation rates and to the chains' high ultimate conformational elongation (*4*). For example, increasing M_w from 50 kg/mol to 5000 kg/mol decreases the critical elongation rate by more than three orders of magnitude and increases the ultimate molecular elongation by two orders of magnitude.

Unfortunately, ultralong backbones undergo chain scission during routine handling because hydrodynamic tension builds up along the backbone to a level that breaks covalent bonds; this "shear degradation" continues until the chains shorten to a point that their valuable effects are lost ($M_w < 1000$ kg/mol) (*3*). Self-assembly of end-associative polymers creates supramolecules that can potentially break and reassociate reversibly, but formation of megasupramolecules ($M_w \geq 5000$ kg/mol) at low concentration has never been realized for two reasons: (i) End-to-end association at low concentration predominantly leads to rings of a small number of chains (*5*), and (ii) the size of the building blocks is limited because end association is disfavored when they are larger than 100 kg/mol (*6*–*8*).

The current study focuses on megasupramolecules soluble in low-polarity fluids, especially in liquid fuels. Transportation relies on such liquids, presenting the risk of explosive combustion in the event of impact, such as in the 1977 Tenerife airport disaster—an otherwise survivable runway collision that claimed 583 lives in the post-crash fireball. Subsequent tests of ultralong, associative polymers [e.g., ICI's "FM-9," > 3000 kg/mol copolymer, 5 mole percent (mol %) carboxyl units] in fuel increased the drop diameter in post-impact mist (*1*, *9*), resulting in a relatively cool, short-lived fire. However, these polymers interfered with engine operation (*10*), and their ultralong backbone—essential for mist control—degraded upon pumping (*3*).

Our goal is to create megasupramolecules at low concentration that behave like ultralong polymers, exhibiting expanded ("self-avoiding") conformation at rest and capable of high elongation under flow (Fig. 1A, right). This is in contrast to the collapsed, inextensible supramolecules formed by long chains with associative groups distributed along their backbone (Fig. 1A, left) (*11*, *12*). To mimic ultralong polymers, association must occur at chain ends and be predominantly pairwise. In contrast to multimeric association (*6*, *8*) that leads to flower-like micelles at low concentration (Fig. 1A, center), recent studies have shown that hydrogen bonding can readily achieve pairwise association for short chains with $M_w \leq 50$ kg/mol (*7*, *13*–*19*). At low concentration, these have no significant rheological effects, consistent with the theory of ring-chain equilibrium (*5*, *20*–*23*); small rings are the predominant species at low concentration (Fig. 1A, center). We realized that using very long chains as the building blocks would disfavor rings, because the entropy cost of closing a ring increases strongly with chain length.

Despite prior reports indicating that end association becomes difficult as chain length increases

[1]Division of Chemistry and Chemical Engineering, California Institute of Technology, Pasadena, CA 91125, USA. [2]Electrochemical Technologies Group, Jet Propulsion Laboratory, Pasadena, CA 91109, USA. [3]Office of the Chief Technologist, Jet Propulsion Laboratory, Pasadena, CA 91109, USA. [4]U.S. Army RDECOM TARDEC, 6501 East 11 Mile Road, Warren, MI 48397, USA.
*These authors contributed equally to this work. **†Corresponding author. E-mail: jakornfield@cheme.caltech.edu**

End-bonded contacts for carbon nanotube transistors with low, size-independent resistance

Qing Cao *et al.*

Science **350**, 68 (2015);
DOI: 10.1126/science.aac8006